

Electronic Supplementary Information for:

Spontaneous Carrier Generation and Low Recombination in High-Efficiency Non-fullerene Solar Cells

Guanqing Zhou¹, Ming Zhang¹, Jinqiu Xu¹, Yankang Yang¹, Tianyu Hao¹, Lei Zhu¹, Libo Zhou¹, Haiming Zhu^{2,*}, Yecheng Zou³, Gang Wei³, Yongming Zhang^{1,3}, Feng Liu^{1,3,*}

¹Frontiers Science Center for Transformative Molecules, In-situ Center for Physical Science, and Center of Hydrogen Science, School of Chemistry and Chemical Engineering, Shanghai Jiao Tong University, Shanghai 200240, P. R. China.

²Department of Chemistry, Zhejiang University, Hangzhou, Zhejiang 310027, P. R. China.

³State Key Laboratory of Fluorinated Functional Membrane Materials and Dongyue Future Hydrogen Energy Materials Company, Zibo, Shandong 256401, P. R. China.

*email: hmzhu@zju.edu.cn (H.Z.); fengliu82@sjtu.edu.cn (F.L.).

Methods

Materials and General Methods: All reagents and chemicals were purchased from commercial sources (Aldrich or Acros) and used without further purification. PM6 and Y6 were purchased from Solarmer company. The number-average molecular weight (M_n) and polydispersity index (PDI) of PM6 were 29.8 kDa and 2.32, respectively.

Device Fabrication: Organic solar cell devices with ITO/PEDOT:PSS/PM6:Y6/PNDIT-F3N-Br/Ag structures were fabricated according to the following procedure. Patterned ITO glass substrates were sequentially cleaned by ultrasonication in acetone, detergent, deionized water and isopropyl alcohol for 15 min each and then dried under dry oven.

Device Characterization: The current-voltage (J - V) curves were measured with Keithley 2400 Source under the illumination of AM 1.5 G irradiation (100 mW cm^{-2}) using a 150 W solar simulator (DM-40S3, SAN-EI ELECTRIC, Japan) in ambient air. The light intensity was determined by a $2 \times 2 \text{ cm}^2$ standardized monosilicon cell (Oriel PN 91150V, Newport, USA.) calibrated by the National Renewable Energy Laboratory (NREL). The external quantum efficiency (EQE) measurement was conducted on a TRACQ-BASIC System using a lock-in amplifier with a monochromator and 500 W xenon lamp. A calibrated silicon detector (PRL-12, Newport, USA) with known photo response was utilized as a reference.

SCLC Mobility Measurements: The electron-only devices fabricated with ITO/ZnO/PM6:Y6/ZnO/Ag structures and hole-only devices were fabricated with ITO/PEDOT:PSS/PM6:Y6/MoO_x/Al structures. The thickness of the active layer is 140 nm. The space charge limited current (SCLC) mobility was calculated according to the Mott-Gurney square law $J = 9\epsilon_r\epsilon_0\mu V^2/8L^3$, where J is the current density, ϵ_r is the relative dielectric constant of the transport medium component, ϵ_0 is the vacuum permittivity, μ is the electron or hole mobility, V is the effective voltage, and L is the thickness of active layer.

Transient photovoltage measurement: The lifetime of carriers can be measured by the transient photovoltage measurement. The background illumination was provided by a normal

LED light source, and pulsed light was provided by arbitrary wave generator (AFG322C, Tektronix). The photovoltage traces were registered by the oscilloscope (AFG322C, Tektronix).

Transient absorption spectroscopy (TA): For femto-second transient absorption spectroscopy, the fundamental output from Yb:KGW laser (1030 nm, 220 fs Gaussian fit, 100 kHz, Light Conversion Ltd.) was separated to two light beam. One was introduced to NOPA (ORPHEUS-N, Light Conversion Ltd.) to produce a certain wavelength for pump beam (here we use 520 and 800 nm, 30 fs pulse duration), the other was focused onto a YAG plate to generate white light continuum as probe beam. The pump and probe overlapped on the sample at a small angle less than 10° . The transmitted probe light from sample was collected by a linear CCD array.

Note S1. Limiting Current Calculation

The limiting current was calculated by the below equations:

$$J_{SC} = q \cdot \int_0^{\infty} EQE_{PV}(E) \cdot \phi_{AM1.5}(E) dE \quad (1)$$

$$J_0 = \frac{q}{EQE_{EL}} \cdot \int_0^{\infty} EQE_{PV}(E) \cdot \phi_{BB}(E) dE \quad (2)$$

the Shockley-Queisser theory, the general quantum efficiency $EQE_{PV}^{SQ}(E)$ can be defined as follow:

$$EQE_{PV}^{SQ}(E) = 1, E \geq E_{gap}; \quad EQE_{PV}^{SQ}(E) = 0, E < E_{gap}. \quad (3)$$

Substituting general quantum efficiency $EQE_{PV}^{SQ}(E)$ (equation 3) in equation 4, then we can get the saturation current in the SQ limit, J_0^{SQ} .

$$J_0^{SQ} = q \cdot \int_{E_{gap}}^{\infty} EQE_{PV}^{SQ}(E) \phi_{BB}(E) dE = q \cdot \int_{E_{gap}}^{\infty} \phi_{BB}(E) dE \quad (4)$$

The expression for J_0 is the Rau's reciprocity relation, where EQE_{EL} is radiative quantum efficiency of the solar cell when charge carriers are injected into the device in dark, and ϕ_{BB} is the black body spectrum.

Note S2. Hole transfer efficiency calculation

As the overall TA kinetics in the blend contains both the intrinsic relaxation of Y6 and HT from Y6 to PM6, the HT rate in PM6:Y6 can be calculated by

$$k_{HT} = k_r - k_0 \quad (5)$$

Where $k_r = 1/\tau_r$, τ_r is the rising time of GSB kinetics at 595 nm, and $k_0 = 1/\tau_0$, τ_0 is the intrinsic relaxation time of Y6 (exciton lifetime of neat Y6 film).

The quantum efficiency (QE) of photoinduced HT (in competition with intrinsic relaxation) can be estimated by

$$QE = k_{HT}/(k_{HT} + k_0) \quad (6)$$

Note S3. Determination of the polaron cross-section and polaron yields

For the chemical doping measurements, the polymer PM6 were solved in chloroform with a concentration of 20 $\mu\text{g/mL}$. Absorption measurements of these solutions filled in Cuvette with a light pass of 1 mm were done with an absorption spectrometer covering the spectral range from 550 to 950 nm. Then, doping different concentration of Y6 from 1-4 wt%. Measurements in between allowed to observe the changes in absorption due to increasing oxidizing without inducing further changes to the solution. Subtraction of the ground state absorption measured in undoped solutions lead to the chemically induced GSB spectra of the investigated polymers. Supplementary Figure S18 shows the differential GSB spectra for doping concentrations from 1 to 4 wt%. Dopant concentration dependence of polaron absorption is shown in Figure S19. Up to a doping ratio of 4 percent a linear increase of the polaron absorption intensities can be observed, suggesting that for each PM6 molecule a single hole polaron is generated. The optical density of the GSB (OD_{polaron}) versus the molecular dopant concentration (C_{dopant}) allows to calculate their molar absorption coefficient ε

$$\varepsilon(\lambda_{\text{probe}}) = \frac{OD_{(\text{probe})}}{C_{\text{dopant}} \cdot x} \quad (7)$$

for the desired wavelength used in the pump probe experiments (cell path length $x = 1$ mm). The measured dopant induced differential optical densities (ΔOD) versus the doping concentration together with linear fitting curves are shown in Supplementary Figure S19 for PM6 at the relevant wavelengths. The resulting polaron cross sections have been calculated according to

$$\sigma_{\text{polaron}}(\lambda_{\text{probe}}) = \ln(10) \cdot \frac{\varepsilon(\lambda_{\text{probe}})}{Na} \quad (8)$$

on the basis of the reasonable assumption that every inserted Y6 molecule resulting in one polaron on the polymer molecule. The number of generated excitons was evaluated by

$$N_{photoexcitations} = \frac{I_{excitation}}{h\omega_{pump}} \bullet (1 - 10^{(-OD_{sample}(\lambda_{pump}))}) \quad (9)$$

With $I_{excitation}$ representing the excitation energy density, $h\omega_{pump}$ the pump photon energy and $OD_{sample}(\lambda_{pump})$ the optical density of the measured sample at the pump wavelength. From the transient absorption signal at the probe wavelength for zero time delay $\frac{\Delta T(\tau\lambda_{probe})}{T}$ the number of generated positive and negative polarons can be evaluated by

$$N_{polarons} = - \frac{1 \log_{10}(1 - \frac{\Delta T(\tau\lambda_{probe})}{T})}{\sigma_{polaron}(\lambda_{probe})} \quad (10)$$

where the denominator accounts for the sum of the contributions to the polaron cross-section from polarons.

The resulting polaron pair yield is then given by

$$\eta_{polaronpair} = \frac{N_{polaron}}{N_{photoexcitation}} \quad (11)$$

Note S4. Exciton annihilation method

The series of fluence dependent decays are globally fit to a rate equation accounting for bimolecular (exciton annihilation) and monomolecular decay pathways, assuming that annihilation destroys both excitons:

$$\frac{dn(t)}{dt} = -kn(t) - \frac{1}{2}\gamma n^2(t) \quad (12)$$

Which has the following solution:

$$n(t) = \frac{n(0)e^{(-kt)}}{1 + \frac{\gamma}{2k}n(0)[1 - e^{(-kt)}]}$$

(13)

Where $n(t)$ is the singlet exciton density as a function of time after the laser excitation, k is the monomolecular decay rate and γ is the singlet-singlet bimolecular exciton annihilation rate. Here the intrinsic monomolecular decay constant, k , is fixed at $6.5 \times 10^9 \text{ s}^{-1}$, extracted from the dilute Y6 film where diffusion and annihilation does not occur. The global fits shown in Figure 5e

account for absolute excitation densities, which are ascertained from the TA signal after accounting for the fluence.

The exciton decays in Figure 5e are well fitted by eq 6, where the only free parameter is the bimolecular rate constant, fit as $1.13 \times 10^{-6} \text{ cm}^3/\text{s}$. The bimolecular rate constant is then used to

$D = \frac{\gamma}{8\pi R}$ determine the 3D exciton diffusion coefficient; where D is the diffusion constant and R

is the effective interaction or annihilation radius of singlet excitons that is the separation at which the annihilation occurs. Spectral overlap of PL and exciton absorption yields a Förster radius for exciton–exciton annihilation of 4.8 nm, which then gives a 3D diffusion coefficient of $9.6 \times 10^{-2} \text{ cm}^2/\text{s}$. The measured exciton diffusion coefficient for solution processed Y6 films is substantially higher than that of most solution-processed organic semiconductors. The exciton diffusion length, $L_D = \sqrt{D\tau}$ is estimated for Y6 as $\sim 39 \text{ nm}$. Here, the intrinsic exciton lifetime, τ , is taken as 153 ps from the dilute film measurement. The TA and TRPL kinetics of dilute Y6 film can be seen in Figure S13.

Note S5. Onsager-Braun Model

The rate equations describing the second mechanism are shown in eq 14, which have the initial conditions that a fraction f of the excitons create spatially separated charges within the pulse length of the excitation and the remaining $(1-f)$ of the excitons create charge-transfer states that decay monomolecularly.

$$\begin{aligned}
 dCT / dt &= -k_{CT \rightarrow GS} CT \\
 dSSC / dt &= -\gamma SSC^{\lambda+1} \\
 dGS / dt &= k_{CT \rightarrow GS} CT + \gamma SSC^{\lambda+1} \\
 CT(t) &= N_0(1-f) \exp(-k_{CT \rightarrow GS} t) \\
 SSC(t) &= (\lambda\gamma t + (fN_0)^{-\lambda})^{-1/\lambda} \\
 GS(t) &= N_0(1-f)(1 - \exp(-k_{CT \rightarrow GS} t)) + N_0 f - ((\lambda\gamma t + (fN_0)^{-\lambda})^{-1/\lambda})
 \end{aligned} \tag{14}$$

Supplementary Figures

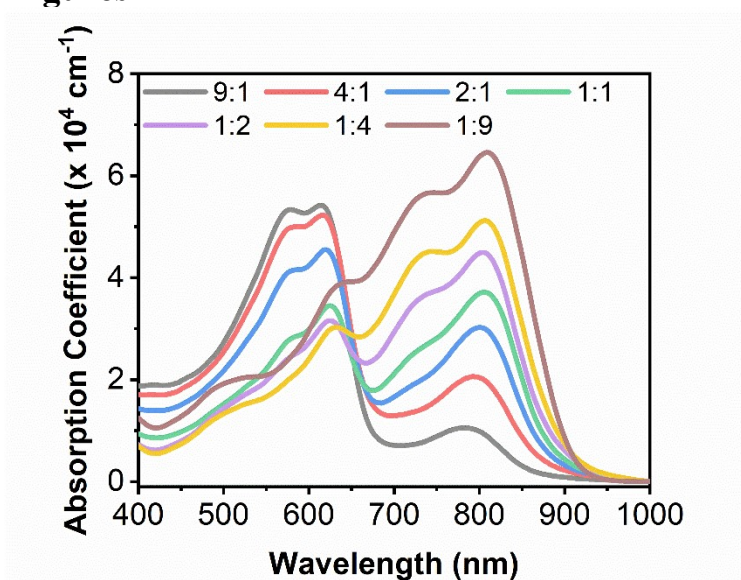


Fig. S1 The absorption spectrum of PM6:Y6 blend films with various composition ratios.

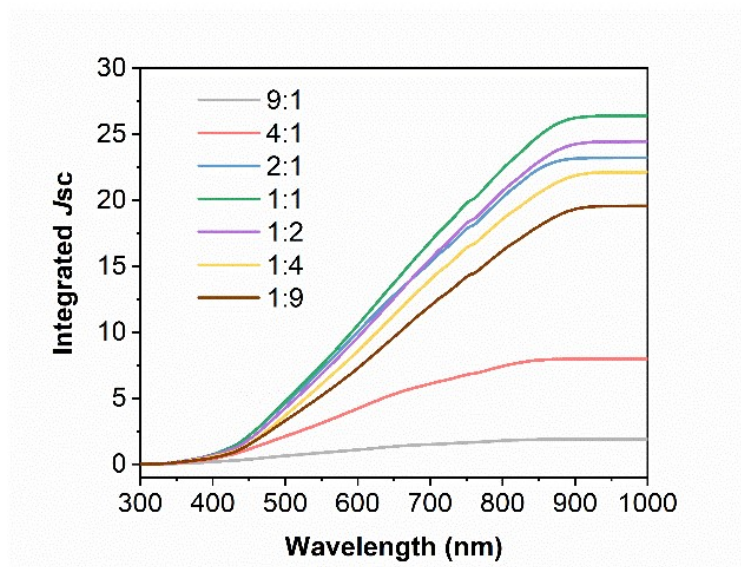


Fig. S2 Integrated J_{sc} of PM6:Y6 blend solar cells with various composition ratios

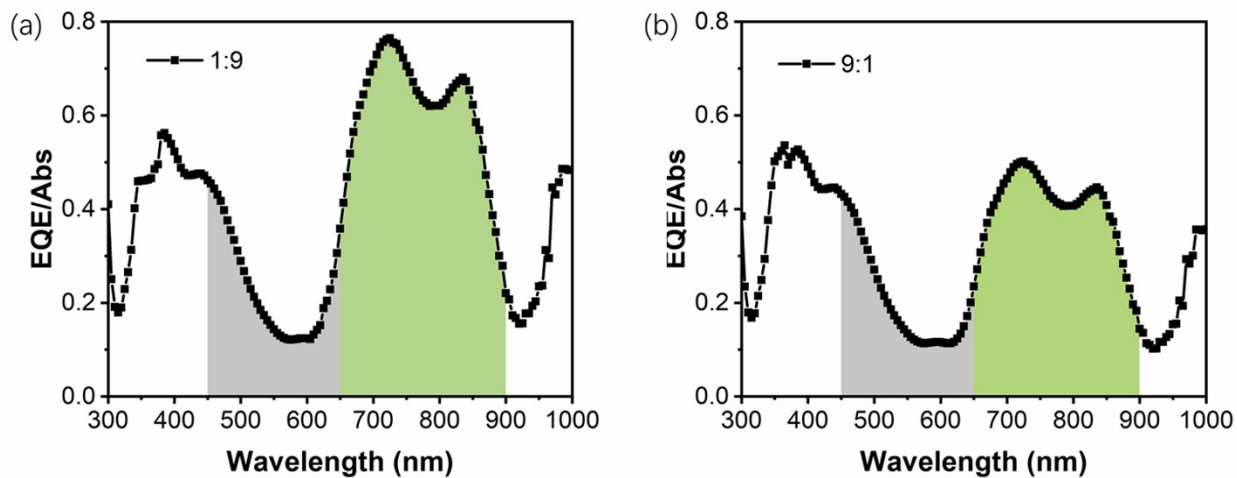


Fig. S3 The EQE/Absorption spectrum of 1:9 and 9:1 PM6:Y6 blend solar cells.

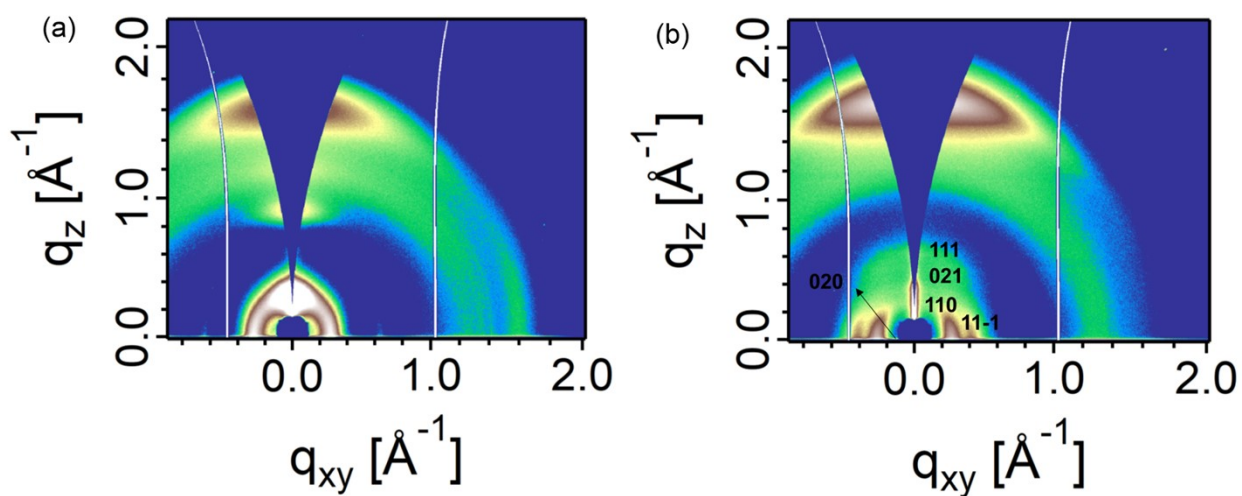


Fig. S4 2D GIWAXS patterns for pure (a) PM6 and (b) Y6 film.

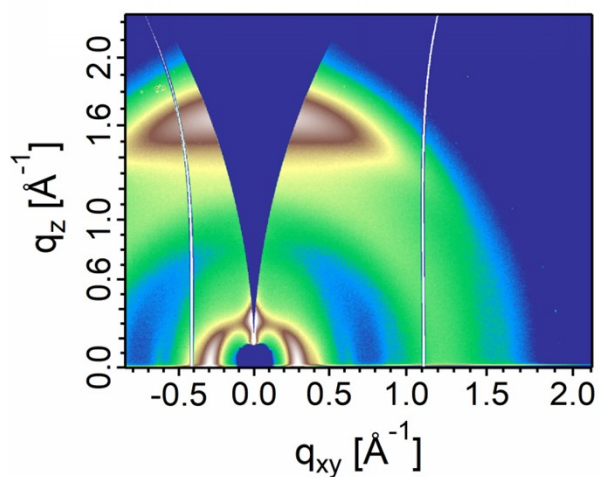


Fig. S5 2D GIWAXS patterns for PM6:Y6 (1:1) blend films.

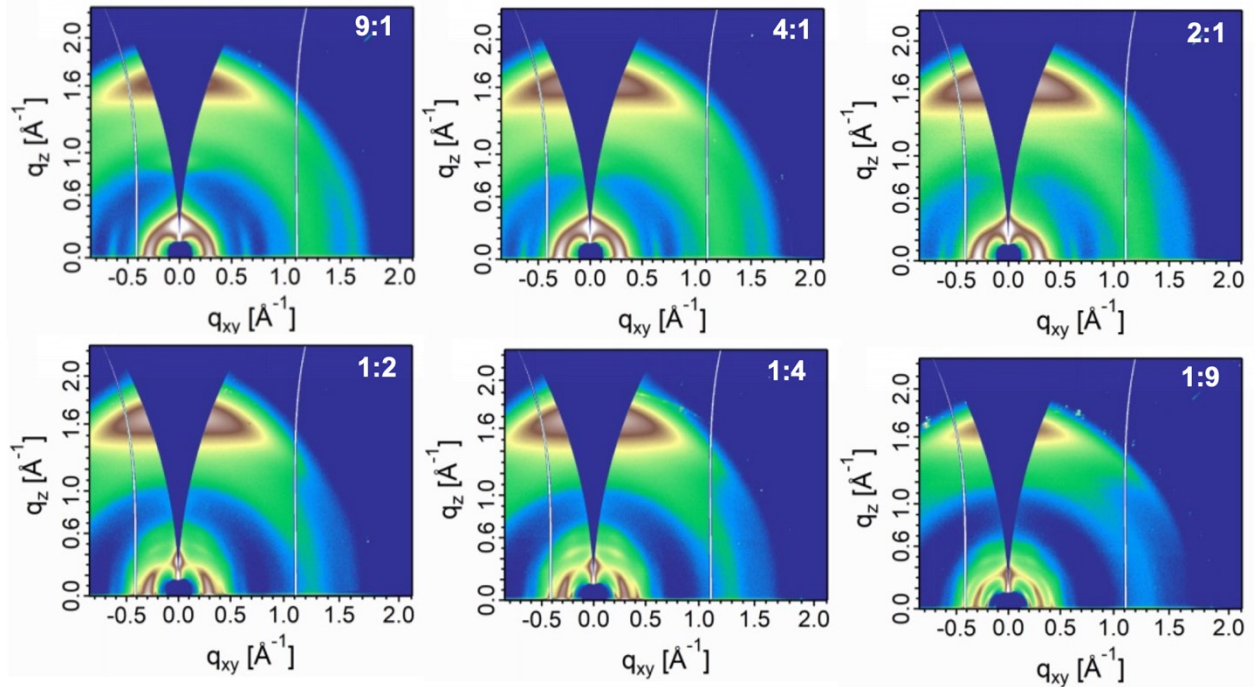


Fig. S6 2D GIWAXS patterns for PM6:Y6 blend solar cells with various composition ratios.

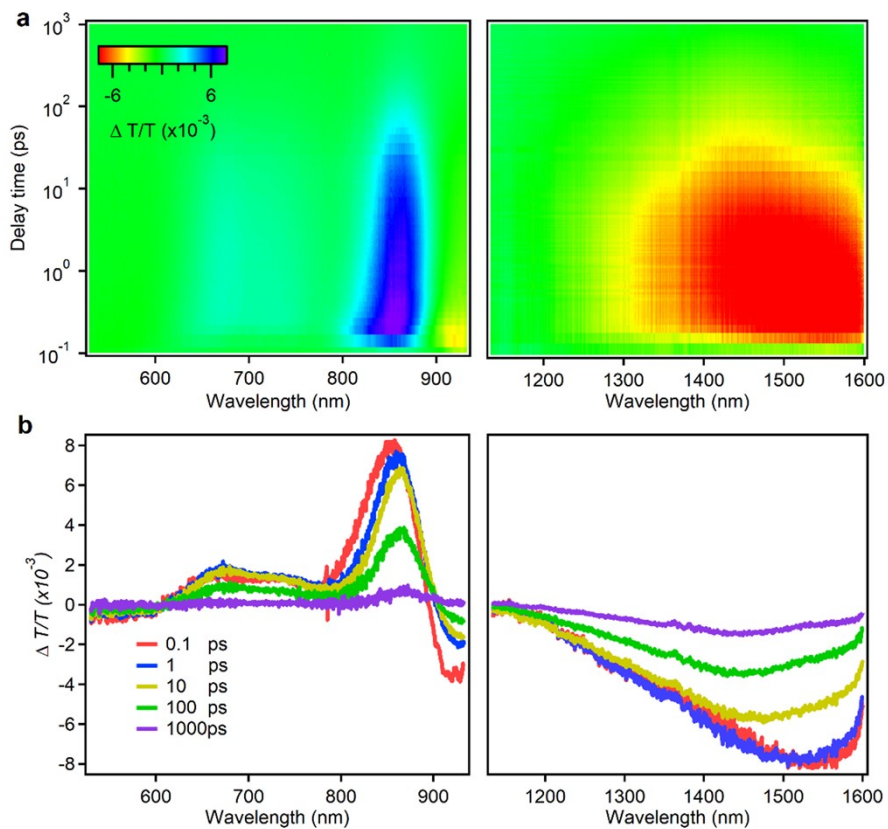


Fig. S7 a, Color plot of TA spectra of neat Y6 film under 800 nm excitation with a fluence below $10 \mu\text{J cm}^{-2}$. b, Representative TA spectra at indicated delay times.

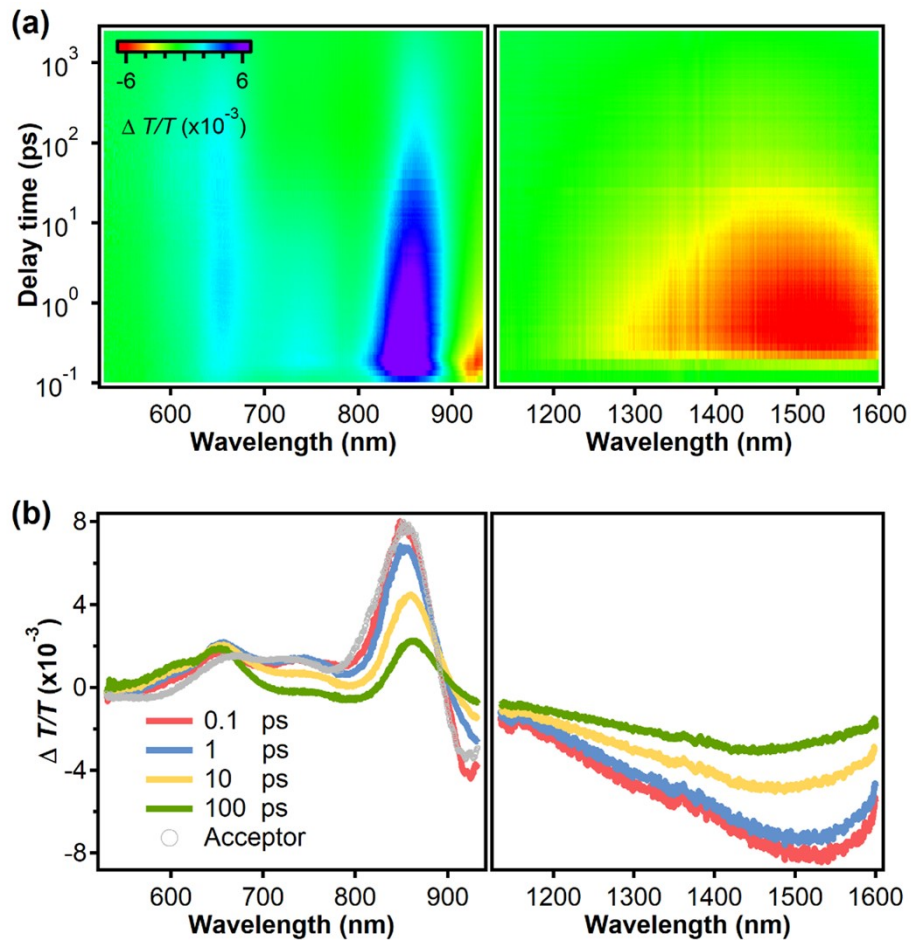


Fig. S8 a, Color plot of TA spectra of PM6:Y6 (1:1) blend films under 750 nm excitation with a fluence below $10 \mu\text{J cm}^{-2}$. b, Representative TA spectra of PM6:Y6 (1:1) at indicated delay times.

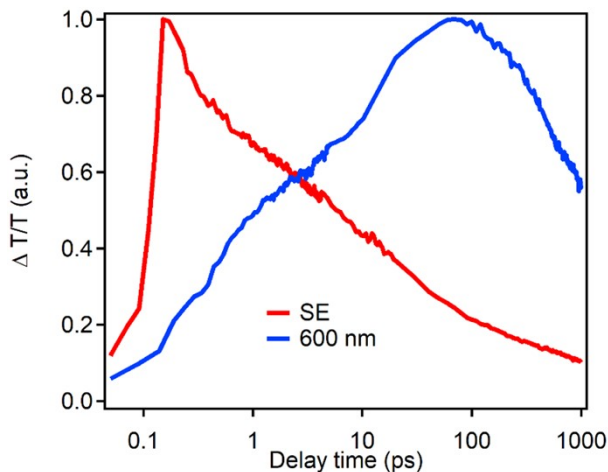
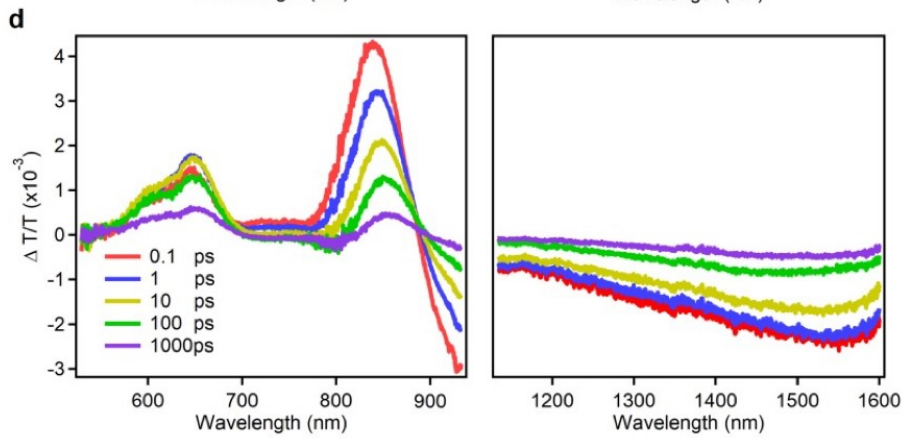
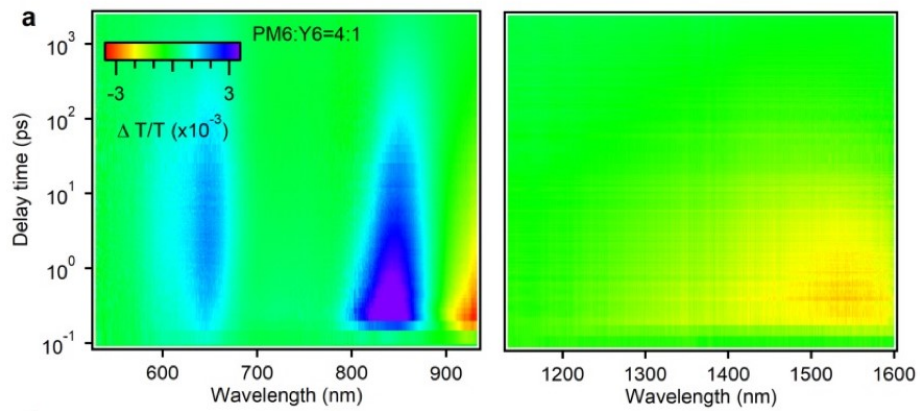
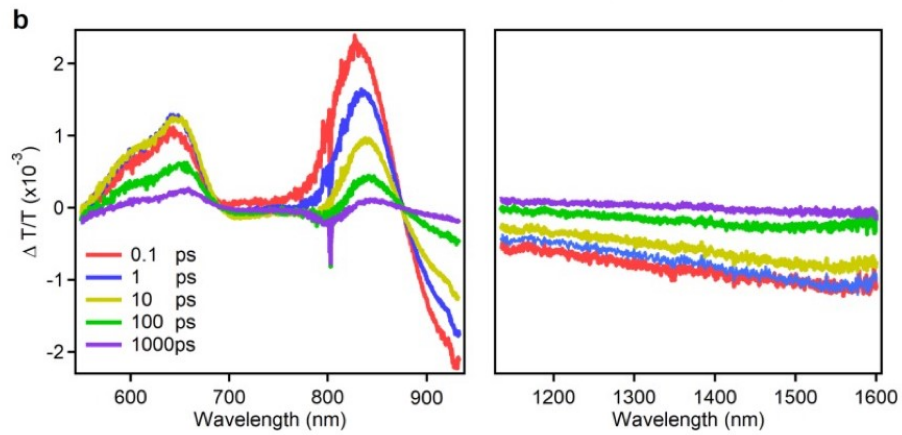
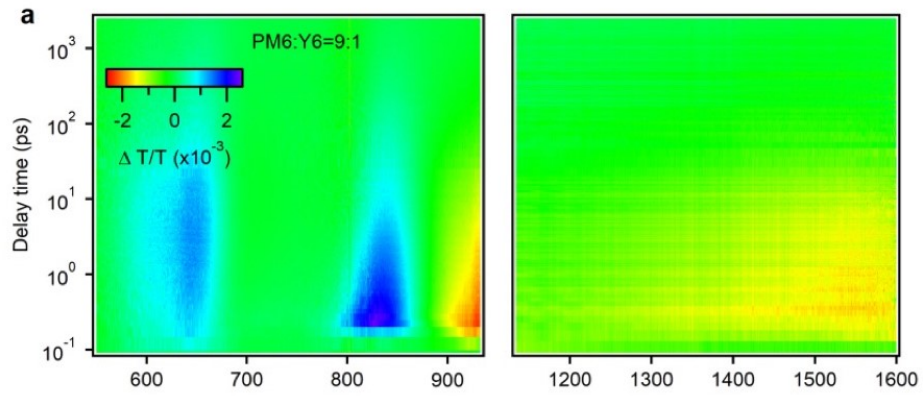
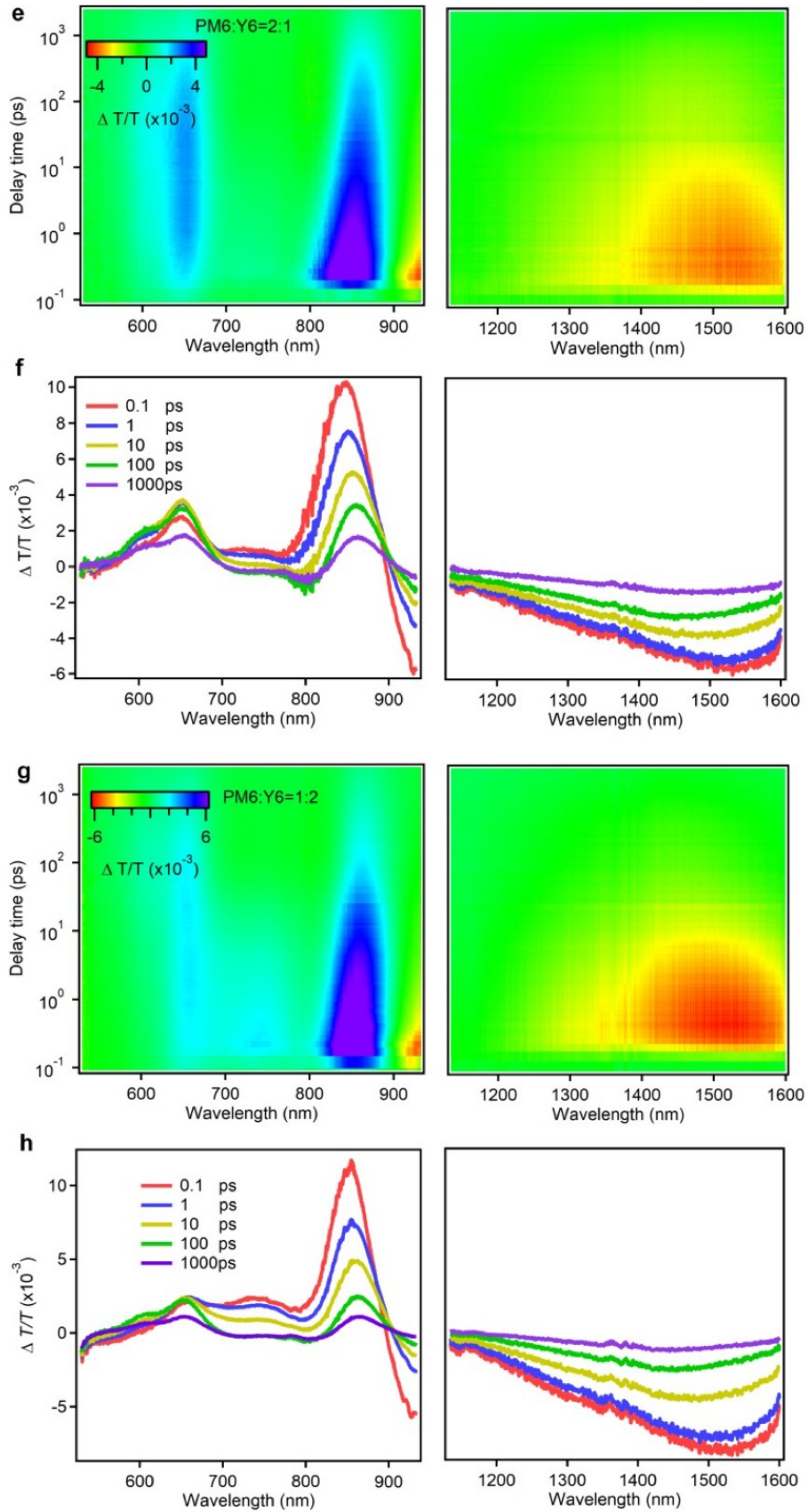


Fig. S10 TA kinetics of PM6 and Y6 in blend film showing photoinduced hole transfer process





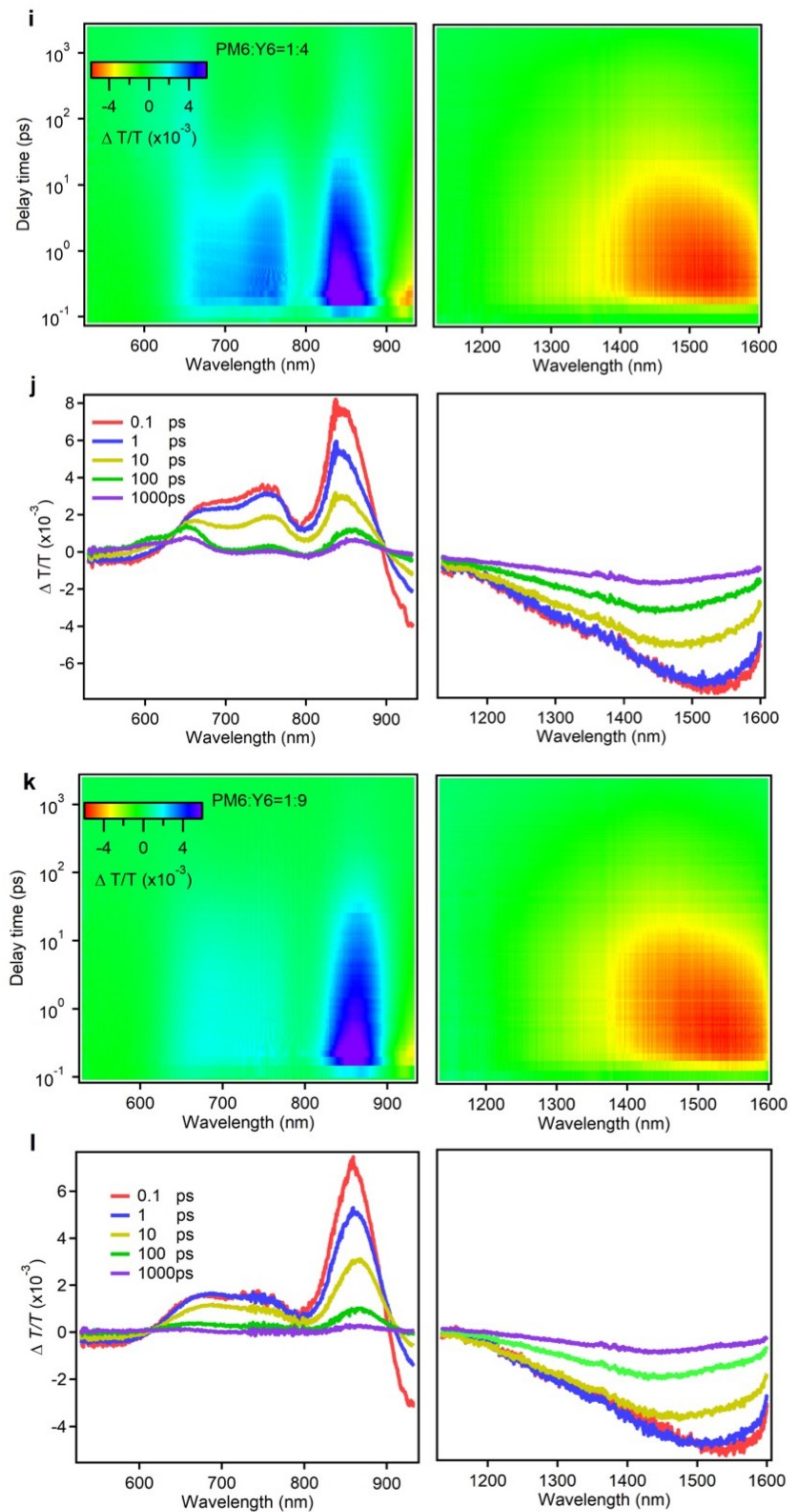


Fig. S11 Color plot of TA spectra of PM6:Y6 blend films in different composition ratios 9:1 (a), 4:1 (c), 2:1 (e), 1:2 (g), 1:4 (i), 1:9 (k) and 1:19 (m) under 750 nm excitation with a fluence below $10 \mu\text{J cm}^{-2}$. b, Representative TA spectra of PM6:Y6 in different composition ratios 9:1 (b), 4:1 (d), 2:1 (f), 1:2 (h), 1:4 (j), 1:9 (l) and 1:19 (n) at indicated delay time.

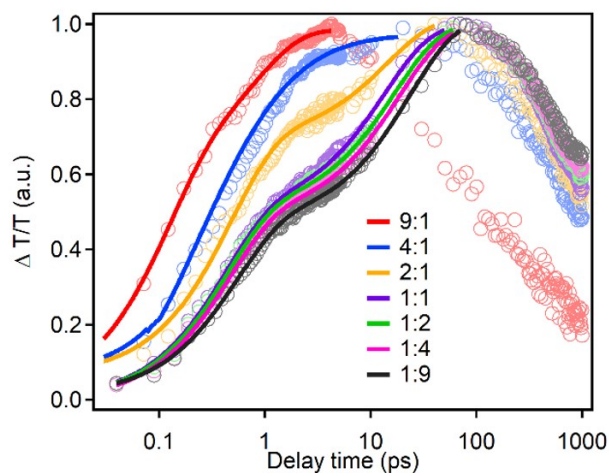


Fig. S12 The fitting hole transfer kinetics of PM6:Y6 blend films in different composition ratios

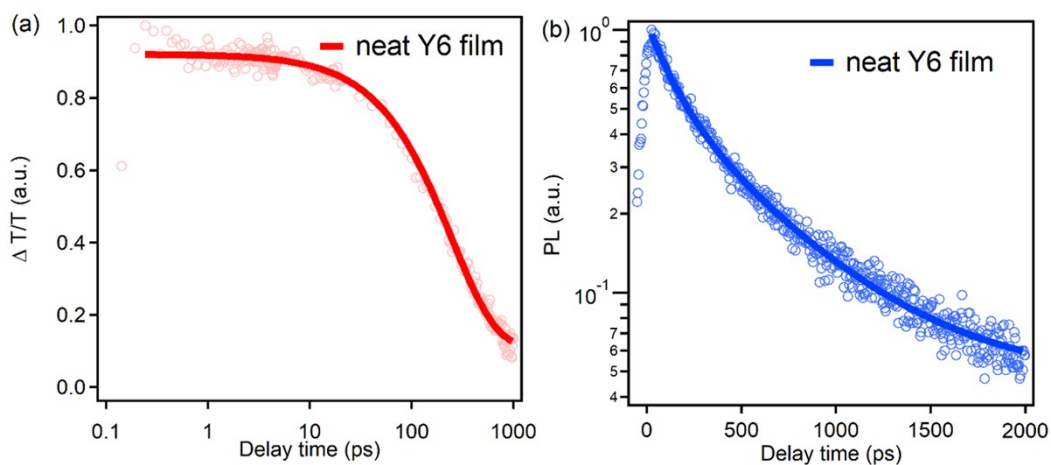


Fig. S13 The (a) TA and (b) TRPL kinetics of neat Y6 film and corresponding fitting results

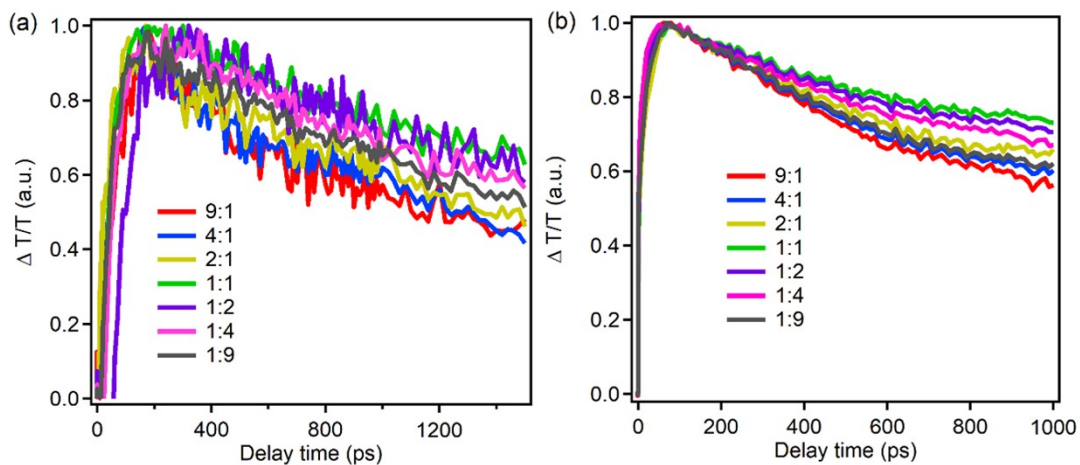


Fig. S14 TA kinetics of PM6:Y6 blend films at 800 nm (a) and 950 nm (b) in different composition ratios.

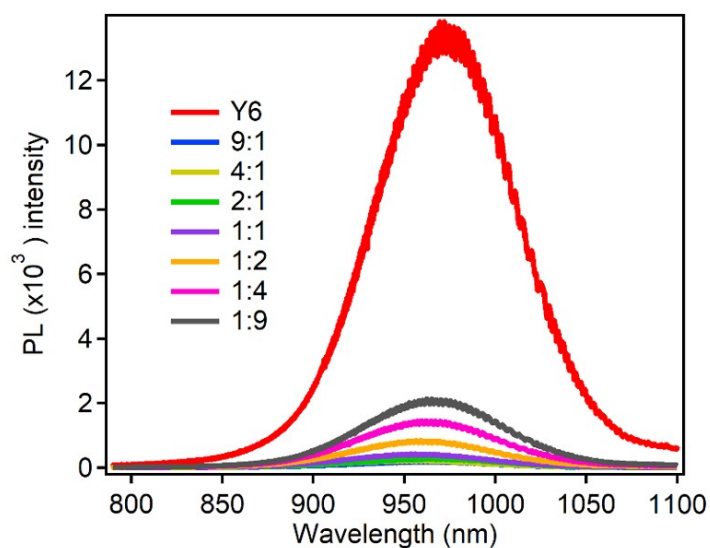


Fig. S15 The steady state PL spectrum of PM6:Y6 blend films and neat Y6 film (excited at 800 nm) in different composition ratios. The PL spectrum was calibrated by steady state absorption of blend films.

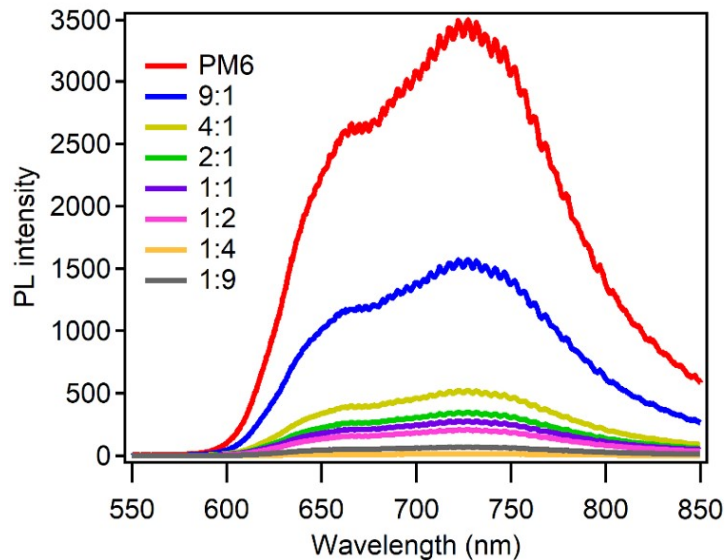


Fig. S16 The PL spectrum of PM6:Y6 blend films and neat PM6 film (excited at 450 nm) in different composition ratios.

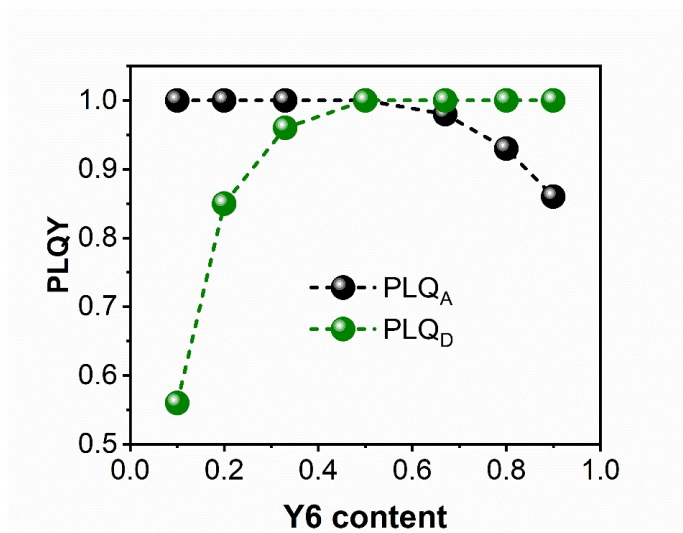


Fig. S17 The PLQY of PM6:Y6 blend films in different composition ratios.

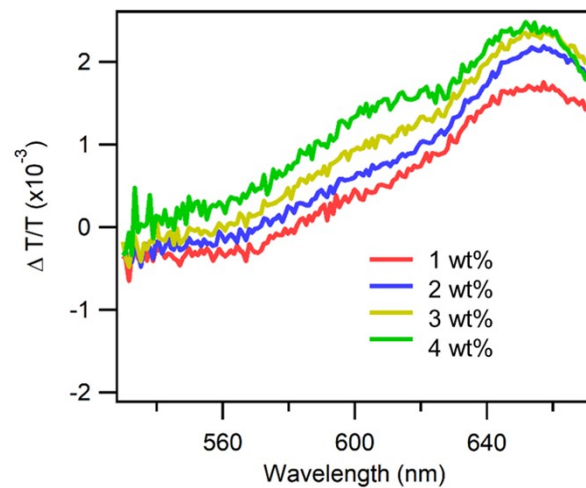


Fig. S18 Polaron spectra. Chemically induced differential GSB for the PM6 with different dopant concentration.

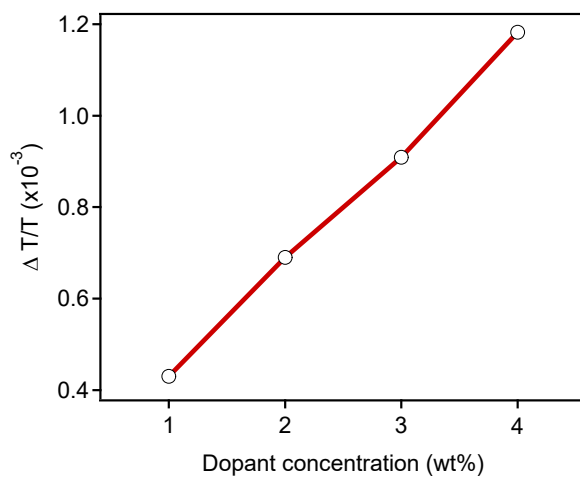


Fig. S19 Dopant concentration dependence of polaron absorption.

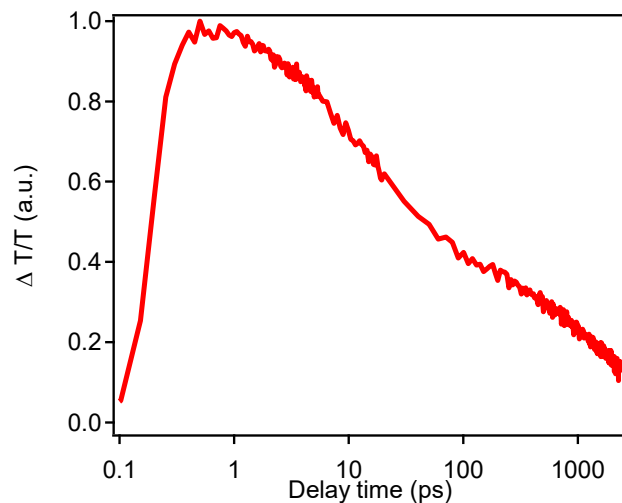


Fig. S20 The TA kinetics at 1450 nm of Y6 neat film.

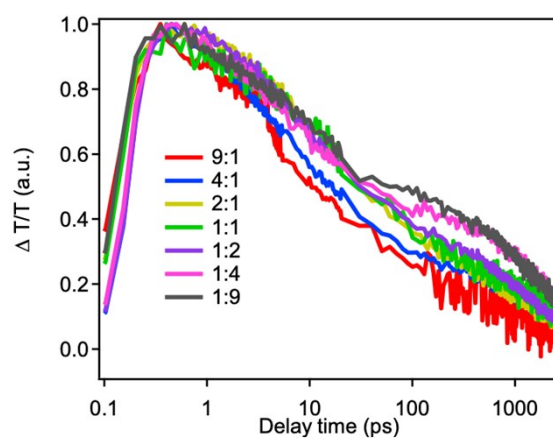


Fig. S21 The TA kinetics at 1450 nm of PM6:Y6 blend films in different composition ratios.

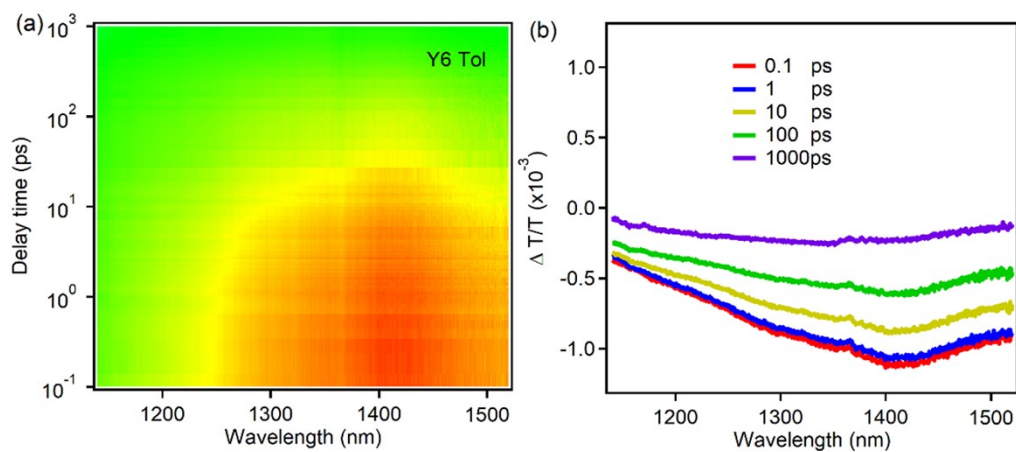


Fig. S22 Color plot of TA spectra and representative TA spectra of Y6 in toluene under 750 nm excitation with a fluence below $10 \mu\text{J cm}^{-2}$.

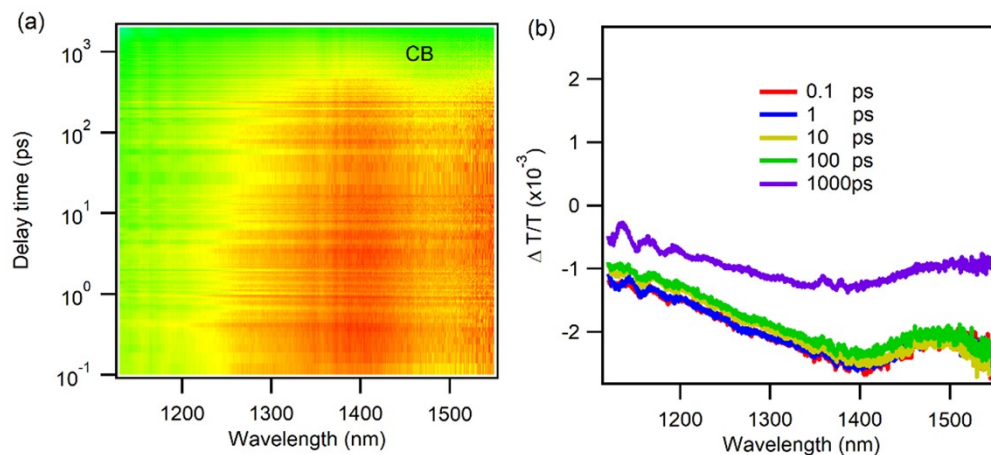


Fig. S23 Color plot of TA spectra and representative TA spectra of Y6 in CB under 750 nm excitation with a fluence below $10 \mu\text{J cm}^{-2}$.

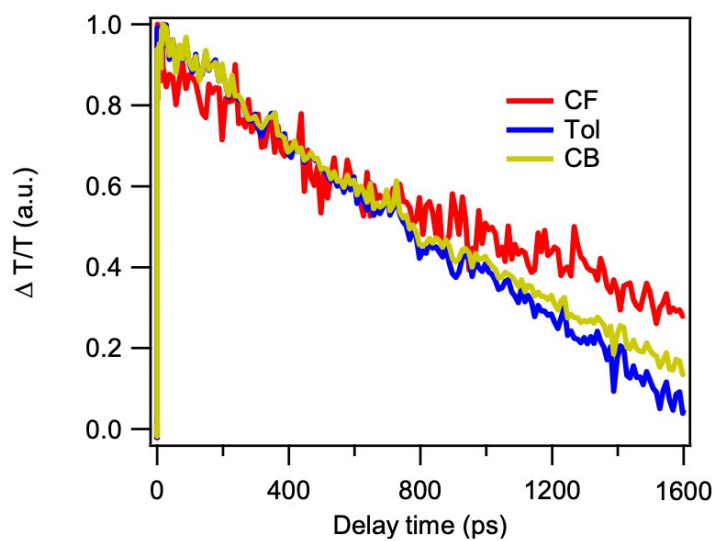


Fig. S24 The polaron kinetics of Y6 in CF, toluene and CB solution.

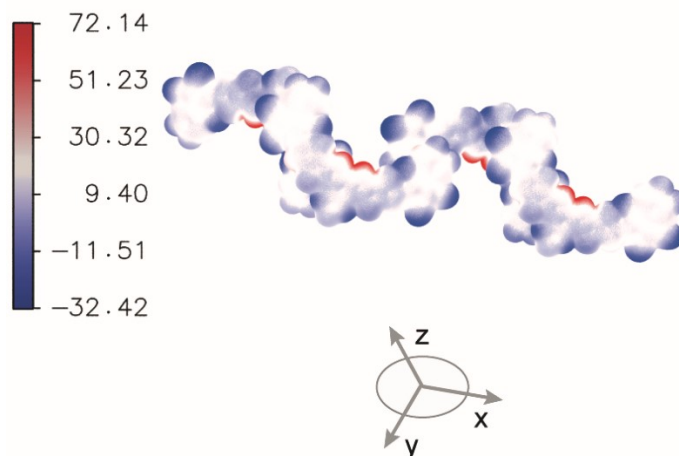


Fig. S25 The static quadrupole moment of Y6 molecules in crystalline field.

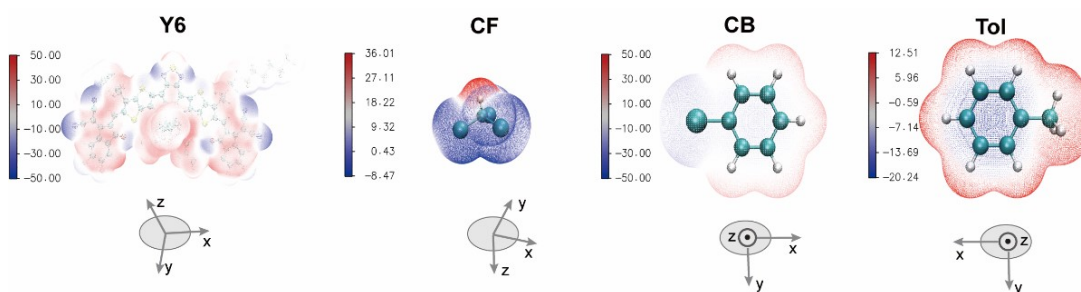


Fig. S26 The electrostatic potential surfaces of Y6, CF, CB and toluene molecules.

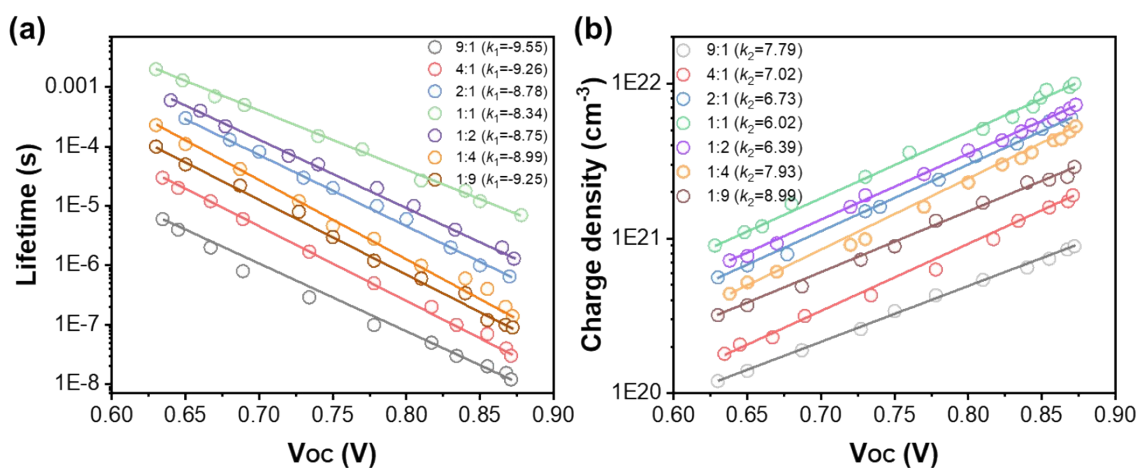


Fig. S27 Lifetime (a) and charge-carriers density (b) under different Voc conditions.

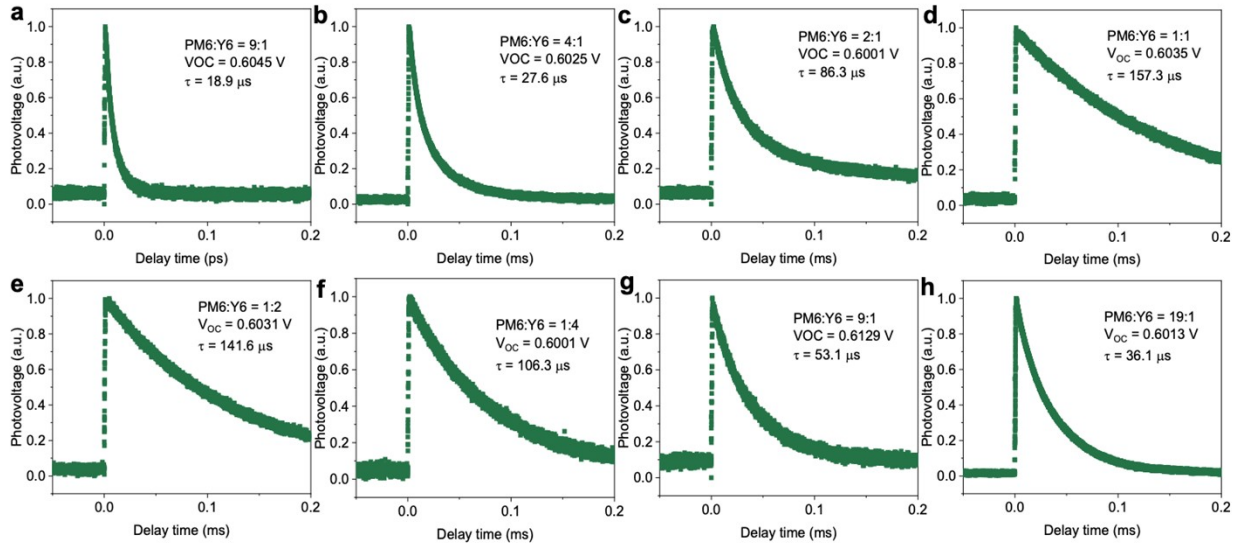


Fig. S28 Transient photovoltage (TPV) measurements of PM6:Y6 based devices under corresponding illumination intensities.

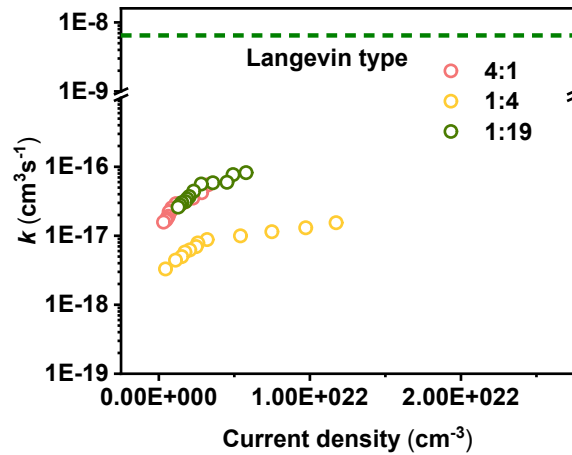


Fig. S29 Current densities at different light intensities according to transient photovoltage (TPV) measurements of the devices.

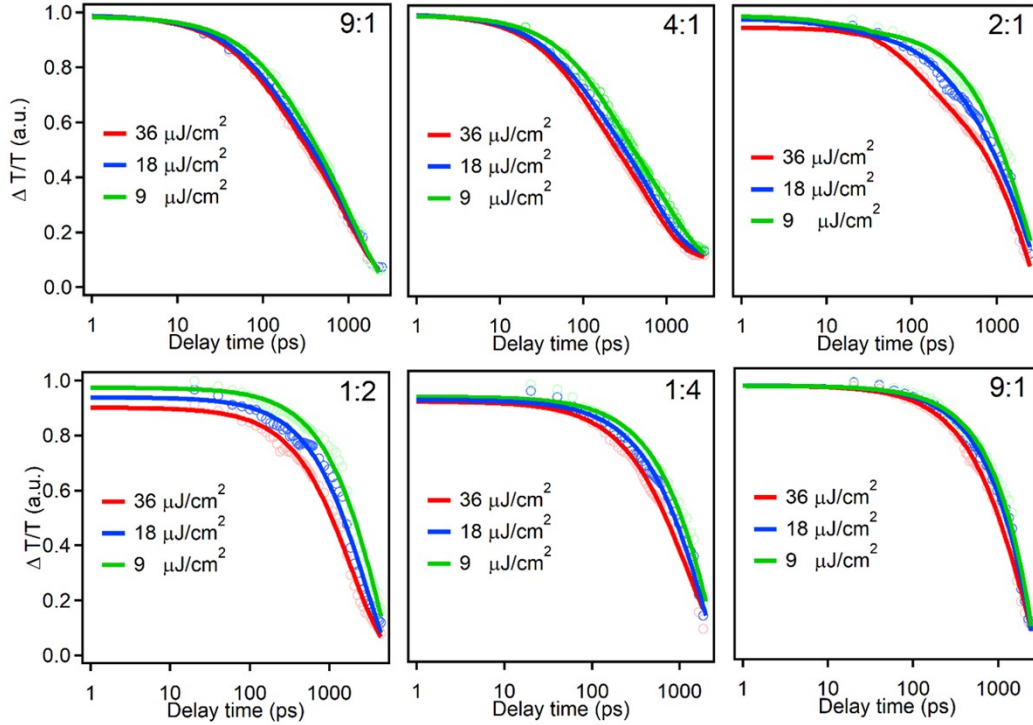


Fig. S30 The polaron kinetics of PM6:Y6 blend films in different composition ratios under indicated pumping fluence.

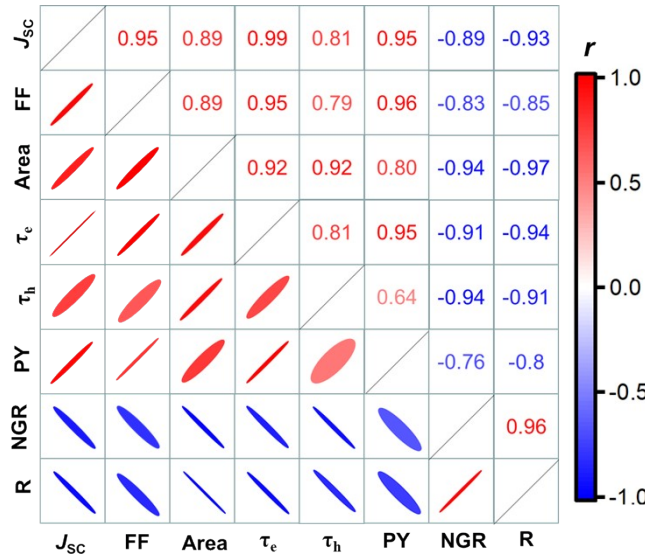


Fig. S31 Confidence ellipse correlation matrix of all parameters including J_{sc} and FF, (010) peak area, electron and hole lifetime, spontaneous polaron yields, nongeminate recombination loss and total recombination loss.

Table S1 The dopant concentration dependence of polaron GSB.

Dopant concentration (wt%)	$\Delta T/T (\times 10^3)$
1	0.43
2	0.69
3	0.91
4	1.18

Table S2 Polaron cross-sections extracted from Supplementary Figure 18,19 at the specific probe wavelengths.

Donor	Probe wavelength/nm	$\epsilon(\text{cm}^2/\text{mol})$	$\sigma(\text{cm}^2)$
PM6	595	1.05×10^8	4.41×10^{-16}

Table S3 Polaron cross-sections extracted from Fig. 4a,b at the specific probe wavelengths.

Acceptor	Probe wavelength/nm	$\epsilon(\text{cm}^2/\text{mol})$	$\sigma(\text{cm}^2)$
Y6	1450	2.05×10^8	7.03×10^{-16}

Table S4 The dipole moments of Y6, CF, CB, toluene molecules.

	Dipole X	Dipole Y	Dipole Z	Dipole
CB	0.788907	0.000003	0.000009	0.788907
CF	-0.000085	-0.000098	0.517006	0.517006
TO	0.136595	-0.019917	0.000048	0.138039
Y6	-0.049690	0.831171	0.607883	1.030939

Table S5 The static quadrupole moment of Y6 molecules in crystalline field.

	Q _{xx}	Q _{yy}	Q _{zz}	Q ₂
Y6	-1609.69	-1214.48	-1126.135	285.95

Table S6 The static quadrupole moment of Y6, CF, CB, toluene molecules.

	Q _{xx}	Q _{yy}	Q _{zz}	Q ₂
CB	-33.62	-30.59	-37.42	5.927
CF	-32.9	-32.91	-31.00	1.911
TO	-27.63	-28.04	-33.43	5.606
Y6	-624.36	-475.39	-467.36	154.667

Table S7 The carrier lifetime, current density and recombination rate at different light intensities according to TPV and TPC measurements of the devices

V_{OC} (V)	τ ($\times 10^{-6}$ s)	Current density ($\times 10^{-9}$ cm ⁻³)	k ($\times 10^{-17}$ cm ³ s ⁻¹)
0.85424	2.014	3.428	13.22
0.84962	2.512	3.361	11.397
0.84269	5.415	3.236	9.654
0.83267	8.232	3.113	8.211
0.82923	11.523	2.927	7.016
0.813945	14.019	2.864	6.352
0.80441	16.203	2.719	5.556
0.79706	18.255	2.582	4.161
0.7869	19.665	2.417	3.748
0.77278	39.130	2.379	2.362
0.69589	51.994	2.152	2.147
0.65045	64.379	2.027	1.879